Nuclear Materials and Energy 49 (2026) 102225



Contents lists available at ScienceDirect

Nuclear Materials and Energy

journal homepage: www.elsevier.com/locate/nme

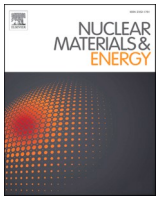

Cleaning rate and uniformity of simultaneous cleaning of two face-to-face mirrors using RF plasma

Yuxian Wen [a,b], Rong Yan [a,*], Chuannan Xuan [a,*], Lei Mu [a], Yuming Liu [a,c], Yuhao Pan [a,b], Zhaohui Wang [a,b], Baoguo Wang [a], Shuyue Sun [a,b], Rui Ding [a], Andrey Litnovsky [d], Junling Chen [a]

[a] Institute of Plasma Physics, Hefei Institutes of Physical Science, Chinese Academy of Sciences, Hefei 230031, Anhui, China
[b] University of Science and Technology of China, Hefei 230026, Anhui, China
[c] Institute of Energy, Hefei Comprehensive National Science Center (Anhui Energy Laboratory), Hefei 230031, Anhui, China
[d] Forschungszentrum Jülich GmbH, Institute of Fusion Energy and Nuclear Waste Management (IFN-1), 52425 Jülich, Germany

ARTICLE INFO

Keywords:
ITER
Diagnostic mirrors
RF plasmacleaning
Reflectivity
Cleaning efficiency

ABSTRACT

Radio frequency (RF) plasma cleaning has been proposed and tested to restore the reflectivity of first mirrors (FMs) which will degrade after long term plasma exposure due to erosion and deposition. While most previous studies have focused on single-mirror cleaning, in realistic situations in ITER, multiple mirrors need to be cleaned simultaneously. This work investigated the cleaning uniformity, optical performance recovery and relevant physical mechanisms of two mirrors placed face to face by RF plasma cleaning with same self-bias. In this work, two 110 mm × 80 mm mirrors arranged face to face were coated with 80 nm-thick Al_2O_3 to simulate beryllium impurity deposition and subjected to 30 h total Ar plasma cleaning at 1 Pa working pressure and −300 V identical self-bias, split into a 9 h preliminary cleaning followed by another 21 h continuous treatment. Mirror cleaning performance was evaluated via mass loss statistics, reflectivity testing (300–1200 nm), SEM, FIB-TEM and EDS characterizations, and the underlying nonuniformity mechanism was further interpreted using particle-in-cell with Monte Carlo collision (PIC-MCC) simulation. Experimental results demonstrate that Al and O contaminations are completely eliminated after full cleaning, and the total reflectivity of both mirrors has basically returned to the original level of the molybdenum substrate. Obvious asymmetric cleaning nonuniformity is observed. Edge/corner material removal is 5–6 times higher than that in the central region, accompanied by excessive substrate sputtering at mirror edges. In addition, the directly opposite area between the two mirrors exhibits higher cleaning efficiency than other positions. PIC-MCC simulations reveal that the ion flux near mirror edges is remarkably intensified to induce rapid edge sputtering, and elevated ionization rate within the opposed gap between two mirrors increases local ion density and ion bombardment flux, accounting for the enhanced material removal at facing regions. The mirror geometric layout is confirmed as a critical factor dominating cleaning uniformity, which provides experimental and simulation references for the structural optimization of multi-mirror RF plasma cleaning modules in future ITER applications.

1. Introduction

In tokamaks, first mirrors (FMs) are key front-end elements for all optical diagnostic systems [1]. Indeed, many of the optical diagnostic systems in ITER use FMs. However, since FM is directly exposed to the plasma, it will be subjected to bombardment by high-energy charged exchange atoms, re-deposition of plasma surface materials (PFMs), as well as long-term radiation (including neutrons, gamma rays, X-rays and ultraviolet). Such complex physical processes can reduce the reflectivity of FMs significantly and affect the accuracy of optical diagnosis [2,3]. Under deposition conditions, the main reason for the deterioration of the reflectivity of FMs is the absorption and interference of the deposition layer. The reflectivity of FMs can be seriously reduced even when the thickness of layer is only 20 nm [4]. The deterioration of reflectivity will result in the inaccuracy of the diagnostics. It is thus important to restore the reflectivity of FMs.

* Corresponding author.
E-mail addresses: yanrong@ipp.ac.cn (R. Yan), chuannan.xuan@ipp.ac.cn (C. Xuan).

https://doi.org/10.1016/j.nme.2026.102225
Received 10 June 2026; Received in revised form 24 August 2026; Accepted 29 September 2026
Available online 30 September 2026
2352-1791/© 2026 The Authors. Published by Elsevier Ltd. This is an open access article under the CC BY-NC-ND license (http://creativecommons.org/licenses/by-nc-nd/4.0/).

Although passive mitigation techniques, such as heating [5] and inflating [6], can reduce the deposition of impurities on the surface of FMs, they still cannot restore the reflectivity of FMs to an ideal value. In order to actively remove the contaminated layer deposited on the surface of FMs and restore its reflectivity, radio frequency (RF) capacitance-coupled plasma has been proposed for cleaning [7,8]. The RF power supply is directly fed into FMs, and plasma is generated on the surface of FMs through capacitive coupling. The ions in the plasma sputter the deposited layer on the mirror surface to remove them and restore the reflectivity of FMs [9]. In the previous experiment of using aluminum (Al) as beryllium (Be) proxy, the argon (Ar) plasma with an ion energy of 150–350 eV at 13.56 MHz radio frequency successfully removed the Al and aluminum oxide (Al_2O_3) deposits on molybdenum (Mo) mirrors with a diameter of 98 mm, while maintaining good optical properties [10]. Meanwhile, due to the different movement speeds of electrons and ions in the plasma, electrons will accumulate on the surface of FMs, forming a sheath near the material surface, which can accelerate the ions [11–14]. In actual situations, however, there are more than 80 FMs in ITER used for all-optical diagnosis [15]. Depending on the specific diagnostic system, either one or two mirrors can be powered simultaneously and cleaned [16–18]. Chenxue Wang et al. conducted the first mirror unit (FMU) dual-mirror cleaning experiment, and discovered that the recovery of reflectivity after double-mirror cleaning varied under different self-bias voltages. However, in this study, the deposited layer on the surface of the mirror after cleaning was not completely removed, and the reflectivity did not fully return to its initial level. It was also observed that there was unevenness in the cleaning process, but no in-depth research was conducted on this issue [19]. The cleaning parameters still need to be further optimized. Furthermore, the cleaning rate and cleaning uniformity are of great significance for the cleaning of FMs in future fusion devices. A high cleaning speed helps to shorten the cleaning time required, while good cleaning uniformity is one of the factors for evaluating the overall recovery of FMs. Therefore, in order to further study the cleaning rate and uniformity of RF plasma cleaning of the FMU, this work conducted a dual-mirror cleaning experiment of the FMU.

In this work, in order to study the cleaning rate and uniformity of cleaning two mirrors simultaneously, we placed the two mirrors face to face, and conducted cleaning experiments in the laboratory using RF plasma. In our previous double-mirror cleaning experiment [19], it was found that a self-bias voltage of −300 V completely removed the deposition layer on the mirror surface and restored its reflectivity. However, the reflectivity of the mirror after cleaning with a low self-bias voltage of −140 V failed to restore. Based on this, in this work, we chose to use the same −300 V self-bias for the dual-mirror cleaning experiment to ensure the effective removal of contaminants and the restoration of the optical performance of the mirrors. The experimental equipment and procedures are as follows: (i) cleaning of two face-to-face mirrors in the FMU at −300 V self-bias for 9 h at the same time and taking them out for testing; (ii) continuing the cleaning of two mirrors for 21 h. Following the introduction, the experiments are described in detail in section 2, including the preparation of mirror samples, the laboratory RF plasma cleaning platform, and the cleaning process and sample characterization. Section 3 introduces the results and discussion of the two face-to-face mirrors cleaning experiment, including the cleaning uniformity (Section 3.1), the role of mirror geometry (Section 3.2). Section 3.3 introduces the simulation method based on particle-grid-Monte Carlo collisions (Particle-In-Cell simulation with Monte Carlo collisions, PIC-MCC), which is used to simulate the plasma motion during the double mirror cleaning process. Finally, the conclusions are presented in section 4.

2. Experiments

In the experiment, small mirror samples with dimensions of 27.5 mm × 20 mm × 5 mm was used for detailed characterization. These samples are composed of polished stainless steel (SS) substrate coated with approximately 500 nm molybdenum (Mo), the surface morphology is shown in Fig. 1(a), presenting dense and uniform columnar crystals. The Nano-crystalline molybdenum (Nc-Mo) coating was applied using a radio-frequency magnetron sputtering coater (Teer CF-800). To simulate the cleaning of Be impurities in ITER, a layer of approximately 80 nm thick Al_2O_3 was deposited on the surface of the Nc-Mo reflector using magnetron sputtering, the thickness and surface morphology of this layer are shown in Fig. 1(c) and 1(d). An Al_2O_3 coating was selected due to its high density and low sputtering yield. However, following the replacement of the ITER first wall material with tungsten, aluminium was no longer the best alternative for deposition, which is a limitation of this work.

To clean two face-to-face mirrors at the same time, the experiment refers to the structure of the FMU [19], in which two mirrors with dimensions of 110 mm × 80 mm are used. The mirrors are respectively labeled as FM (First Mirror) and SM (Second Mirror). As shown in Fig. 2 (b), each mirror is composed of 16 small mirror samples. The FM and SM are arranged in parallel, at an Angle of about 45° relative to the horizontal direction, and are secured by two aluminum alloy mounting plates. The vertical distance between FM and SM is approximately 95 mm, as shown in Fig. 2(a).

The two face-to-face mirrors cleaning experiment was carried out on a laboratory RF plasma cleaning platform, as shown in Fig. 3. The device includes a gas extraction system, a gas supply system, two RF power supply systems and a vacuum chamber. Among them, each RF power supply system consists of an RF power source and an RF matcher. Since the experimental platform used in this study does not have a phase monitoring and control module, the influence of the RF phase relationship on the experiment was not considered in this work. The operating frequencies of both RF sources are 13.56 MHz. The RF matcher is connected to the mirror through an RG 393 cable with a length of 0.3 m. Its characteristic impedance is 50 Ω, and the power attenuation coefficient on the cable is approximately 0.816 dB.

During the experiment, the vacuum chamber was first evacuated to a vacuum level of 10^{-3} Pa using the vacuum pumping system. Subsequently, Ar gas was injected into the vacuum chamber through the gas supply system to maintain the working pressure at 1 Pa. Ar was selected as the working gas because it is an inert gas, which can prevent chemical reactions with the mirror surface or the deposition layer. At the same time, its relatively high atomic mass enables efficient sputtering removal of the Al_2O_3 layer. During the cleaning process, the RF source was connected to the corresponding mirror via an RF matching box. When a RF electric field is applied, the Ar gas is ionized, and the entire vacuum chamber is filled with plasma. However, in the asymmetric capacitively coupled discharge configuration of this experiment, due to the significant difference in area between the RF electrode (mirror) and the grounded electrode (vacuum chamber wall), the RF voltage is mainly concentrated on the smaller electrode side, resulting in a significantly negative self-bias voltage. This self-bias voltage drives positive ions to accelerate and bombard the mirror. The FM and SM were placed in the open top sample box, as shown in Fig. 2(b), and were electrically insulated from the sample box.

During cleaning, the two mirrors were connected to the two RF power supply systems respectively. Table 1 lists the cleaning parameters. The power in Table 1 is the output power of the RF power supply. In the previous experiments in this laboratory [19], it was discovered that when the power of both RF power sources exceeded 63 W, the plasma began to become unstable. Visual inspection revealed that arc discharges appeared on the surfaces of the two mirrors and around them in the FMU. The self-bias voltages displayed by RF matching units A and B were −398 V and −439 V respectively. The experiment revealed that both reducing the working pressure and the self-bias voltage could cause the arc to disappear. Furthermore, we found that cleaning at a self-bias voltage of −300 V could completely remove the contaminants on the mirror surface and restore its reflectivity. However, after cleaning with a

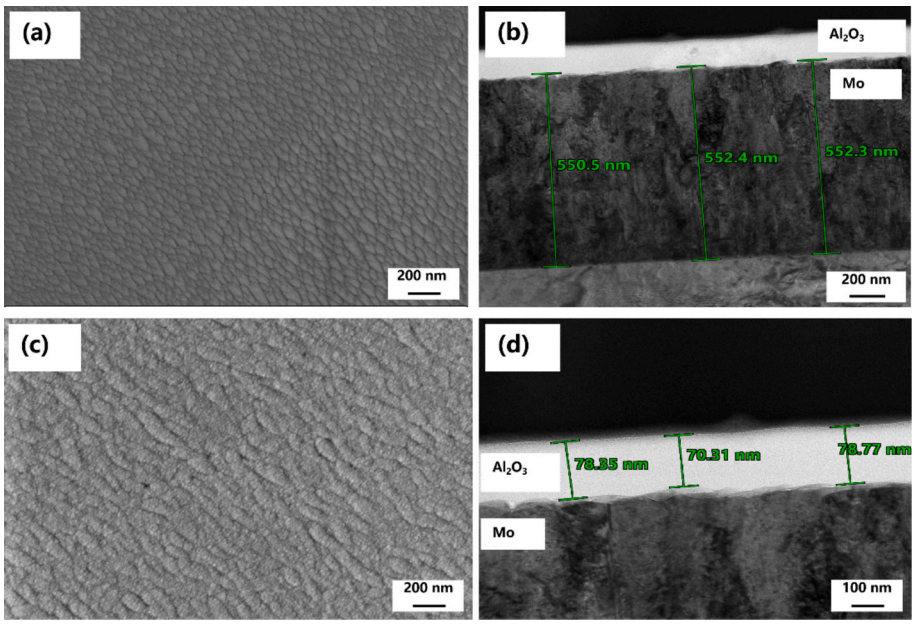

Fig. 1. (a) SEM image of the sample surface after Mo coating; (b) Test results of the sample after Mo coating by FIB-TEM; (c) SEM image of the sample surface after Al_2O_3 coating; (d) Test results of the sample after Al_2O_3 coating by FIB-TEM.

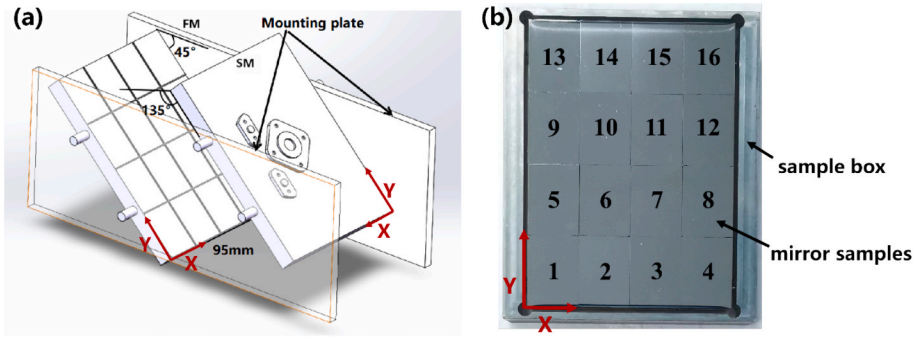

Fig. 2. (a) The FM and SM in the FMU; (b) sixteen small-sized mirror samples assembled on the FM and SM.

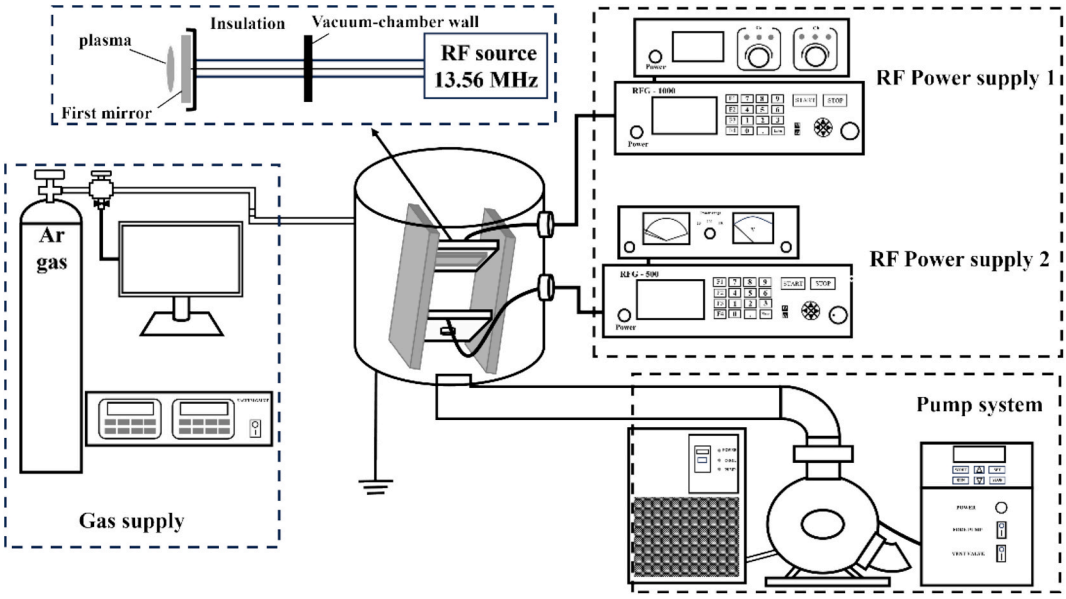

Fig. 3. Schematic diagram of RF plasma cleaning platform.

Table 1
Parameters for plasma cleaning of FM and SM.

	Mirrors	Parameters			
		Pressure (Pa)	Power (W)	Self-bias (V)	Time (h)
Two face-to-face mirrors cleaning	FM	1	40	−300	30(9 + 21)
	SM	1	25	−300	30(9 + 21)

low self-bias voltage of −140 V, the reflectivity of the mirror failed to restore. Therefore, considering all factors, we chose to conduct the dual-mirror cleaning experiment using the same −300 V self-bias as in the previous experiments to ensure the effective removal of contaminants and the restoration of the optical performance of the mirror. During the experiment, the self-bias voltage was achieved by manually adjusting the output power of the RF power source, and its value was directly displayed on the RF matcher panel. Based on previous experiments [19], when cleaning a single mirror under the same cleaning conditions as this experiment, it takes 9 h to completely remove a 30 nm thick Al_2O_3 layer. Due to the thicker Al_2O_3 deposition layer in this experiment, to ensure that all the deposition layers on the FM and SM surfaces are thoroughly removed and the optical properties are restored, we conservatively chose a total cleaning time of 30 h.

A variety of tests were conducted before and after cleaning to determine the reflectivity, quality, surface morphology, elemental composition of the mirror samples on the FM and SM, as well as the thickness of the Al_2O_3 deposition layer on the sample surfaces. The thickness of the Al_2O_3 deposition layer was determined by transmission electron microscope (FIB-TEM, Helios G4 UX) equipped with a focused ion beam scanning. The surface morphology was investigated using a scanning electron microscope (SEM, Zeiss Sigma 300). For the composition analysis, the mirror samples were characterized using energy dispersive spectroscopy (EDS, OXFORD X-Max^N) equipped on the Sigma 300, and the detection depth of the composition analysis was about 1 μm. The total reflectivity and the diffuse reflectivity was measured using an ultraviolet–Visible-near-infrared spectrophotometer (Shimadzu 3700 DUV) in the wavelength range of 300–1200 nm. The mass of the mirror samples was measured using an electronic balance (Sartorius SQP) with an accuracy of 10^{-5} g.

3. Results and discussion

3.1. Cleaning uniformity

After 30 h of cleaning, the SEM images of different samples on the two mirrors are shown in Fig. 4. It can be seen that the surface morphology of the mirror samples changed significantly compared with that before cleaning. After cleaning, the dense rod-like stack on the FM and SM surfaces as shown in Fig. 1(c) disappears, and the surface topography appears pits or dents, and the whole surface is uneven, as shown in Fig. 4. Furthermore, the degree of surface damage varies in different areas of the mirror: the edge area shows more severe pits and depressions, while the central area has relatively less change in surface morphology. This might be caused by excessive sputtering (The Al_2O_3 coating was cleaned thoroughly, and the Mo substrate was then subjected to further sputtering) during the later stage of plasma cleaning. Therefore, we cannot determine exactly when the cleaning process has reached its completion.

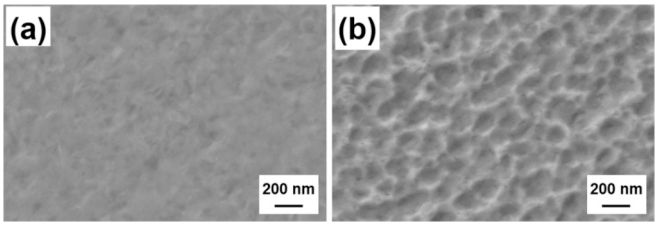

Fig. 4. (a) SEM image of sample 10 on the FM after 30-hours cleaning, with a mass loss of 0.86 mg; (b) SEM image of sample 13 on the SM after 30-hours cleaning, with a mass loss of 6.17 mg.

The EDS results of some samples on the FM and SM surfaces before and after cleaning are shown in Table 2, which showed that after all 30 h of cleaning, Al and O elements were completely removed from FM and SM surfaces.

In this study, no surface roughness measurement was conducted. Therefore, the assessment of optical performance recovery was mainly based on reflectivity measurements. Since the reflectivity recovery levels of samples at various positions were similar after the experiment, and the surface deposition layers had been completely removed—only excessive sputtering occurred in the edge regions—samples 1, 4, 5, 6, 7, and 8 from representative central and edge locations were selected for reflectivity measurements. The total reflectivity and diffuse reflectivity of samples 1, 4, 5, 6, 7, 8 after cleaning on FM and SM is shown in Figs. 5 and 6, which is represented by different symbols. Combined with the reflectivity before cleaning represented by the red solid line and the reflectivity of the initial Mo mirror represented by the black solid line, it can be found that the total reflectivity of the samples at these positions basically recovered after cleaning, among which the total reflectivity range of the former at 300 nm wavelength is 66%–70%, and the latter is 58%–69%. Moreover, the diffuse reflectivity of each sample after cleaning has increased, which might be caused by excessive sputtering. Furthermore, in order to more intuitively demonstrate the recovery of the mirror surface performance after cleaning, the total reflectivity of the same sample before and after 30 h of cleaning is shown in Fig. 7. It can be observed that the total reflectivity of both samples returned to the initial Mo mirror level after cleaning, which proves that the performance of the mirrors has been restored after the cleaning process.

After cleaning for 9 h first, the region close to the boundary of the mirror exhibited metallic luster. The deposition layer still existed in the region inside the mirror, as shown in Fig. 8(a). After cleaning for the first 9 h, a visual inspection revealed that the edge area of the mirror surface presented a metallic color, while the center area remained darker. The significant visual difference between the two indicated that there might be unevenness in the cleaning process. Therefore, we decided to continue the cleaning for another 21 h to ensure that the deposit layer was completely removed throughout the entire mirror surface. After 30 h of cleaning, the EDS results of the samples showed that the Al and O elements in the surface composition of the mirrors were both 0%, which proves that the Al_2O_3 deposition on the surface of the two mirrors was removed completely. Due to the observation with the naked eye revealing uneven areas of different depths at the edge of the reflector, EDS tests were conducted on two locations, L1 and L2, on the surface of sample No. 1 on the FM, as shown in Fig. 8(b). The results are presented in Fig. 8(c). The test results revealed that the mass percentage of Mo element at point L1 was approximately 3.03%, and a large amount of iron (Fe) and other sample base elements were found. At the L2 point, the mass percentage of Mo element is 100% and no other elements were detected. This indicates that during the cleaning process, the cleaning efficiency at the edges of the first and second mirrors were higher than in other areas, and the Ar plasma excessively sputtered the Mo mirror after 30 h of cleaning.

The FIB-TEM test results in Fig. 9 revealed that no Mo layer was observed at L1, while a Mo layer with a thickness of approximately 277.6 nm was observed at L2. This indicates that the net material removal at the edge is significantly higher. Although theoretically, there might be an influence of cross-redeposition between the two mirrors in the dual-mirror configuration, as shown in Fig. 9, the FIB-TEM results indicate that the original Mo layer at the edge L1 point has been completely removed. Such a large amount of material loss is difficult to

Table 2
EDS results of some samples on FM and SM before and after 30-hours cleaning.

Number		FM-4	FM-7	FM-10	FM-13	SM-1	SM-6	SM-11	SM-16
Before cleaning	O (Wt.%)	27.24	30.56	30.41	26.25	28.62	27.52	31.24	27.77
	Al (Wt.%)	20.87	25.07	25.03	21.10	22.99	23.04	26.86	22.63
	Mo (Wt.%)	51.90	44.37	44.57	52.55	48.39	49.44	41.90	49.60
After cleaning	O (Wt.%)	0	0	0	0	0	0	0	0
	Al (Wt.%)	0	0	0	0	0	0	0	0
	Mo (Wt.%)	100	100	100	100	100	100	100	100

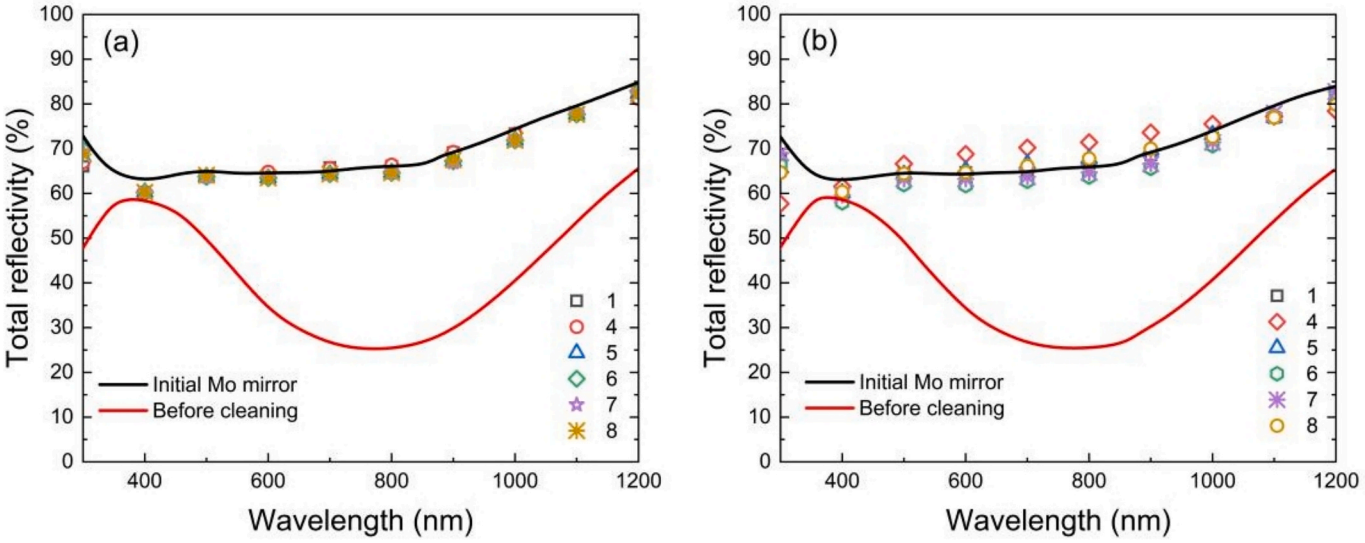

Fig. 5. The total reflectivity of the sample at six typical positions on (a) FM and (b) SM after 30 h of cleaning.

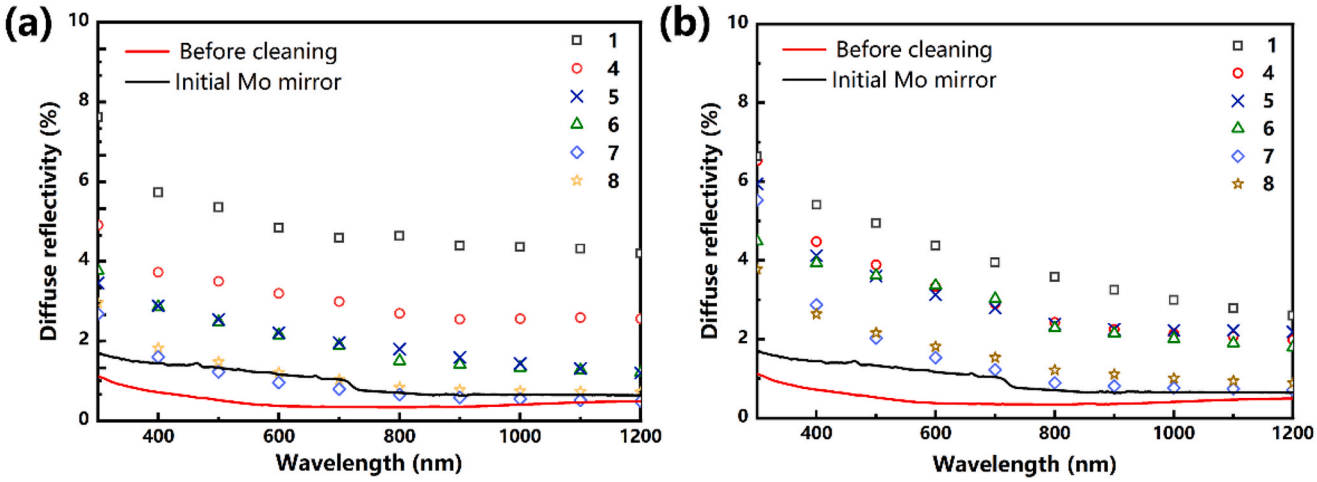

Fig. 6. The diffuse reflectivity of the sample at six typical positions on (a) FM and (b) SM after 30 h of cleaning.

be fully explained by the re-deposition effect even when considering it.

Razdobarin et al. numerically simulated the distribution of the average potential in the gap between the mirror and the ground electrode as the RF power supply electrode [7]. Their results indicate that both the sputtering rate and the calculated ion current density increase near the mirror edge. This suggests that the ion flux distribution is a key factor affecting the uniformity of sputtering in capacitive coupling radio frequency discharge. To verify whether a similar mechanism also exists in the dual-mirror configuration of this experiment, we conducted PIC-MCC simulations to calculate the ion flux distribution under the experimental conditions. The detailed settings of the simulation and the result analysis will be further elaborated in Section 3.3.

3.2. *The role of mirror geometry*

In this study, the mass loss was used as the primary indicator for evaluating the cleaning rate. This method has a good indicative significance when the deposition layer has not been completely removed and no substrate sputtering has occurred. However, due to the uneven cleaning in the edge area compared to the center area, when the deposition layer in the edge area is completely removed and transitional sputtering occurs, the mass loss will include both the removal of the deposition layer and the loss of the substrate material. Therefore, it cannot be directly equivalent to the equivalent removal rate of the deposition layer. Nevertheless, the mass loss can still be used to

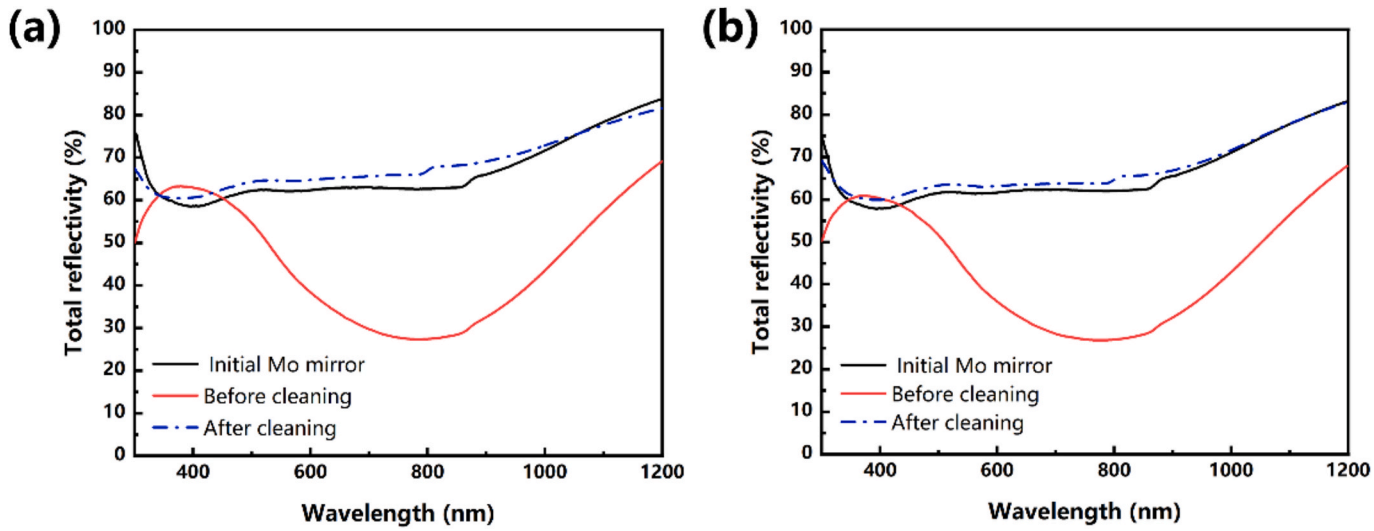

Fig. 7. The total reflectivity of sample 10 on (a) FM and (b) SM before and after 30 h of cleaning.

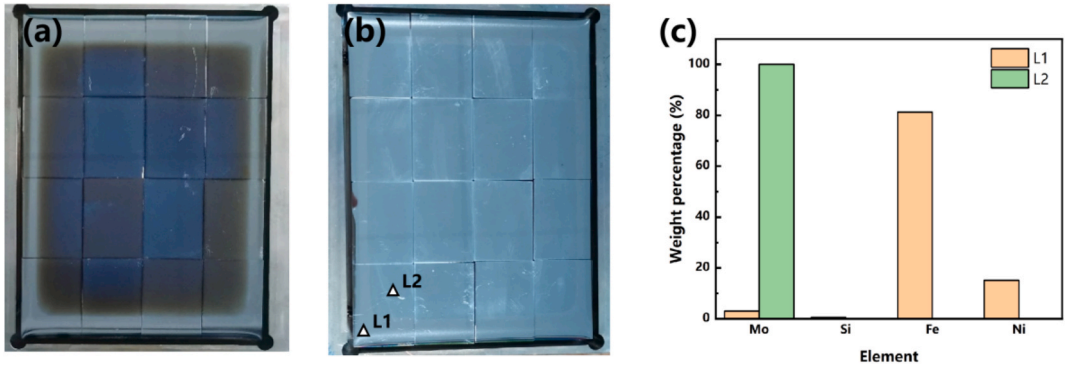

Fig. 8. (a) Macroscopic morphology of the FM surface after 9 h of cleaning; (b) Macroscopic morphology of the FM surface after 30 h of cleaning; (c) EDS test results of a part of Sample 1 on the FM.

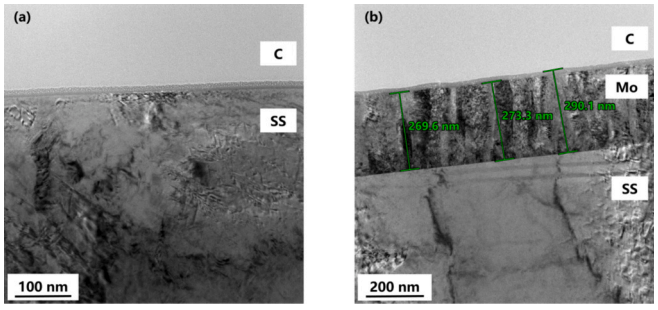

Fig. 9. FIB-TEM images of (a) L1; (b) L2 of sample 1 on the FM.

qualitatively reflect the cleaning non-uniformity. Specifically, during the first 9 h of cleaning, most sample surfaces still retain the Al_2O_3 deposition layer. At this time, the contribution of substrate sputtering is relatively small, and the distribution of mass loss can effectively reflect the differences in cleaning rates in different areas. Moreover, the ion flux distribution obtained from the PIC-MCC simulation is consistent with the overall trend of the mass loss distribution, further supporting the effectiveness of mass loss in qualitatively reflecting non-uniformity.

The mass loss of the samples on the FM and SM before and after different cleaning times is shown in Fig. 10. After calculation, the average mass loss rates of FM and SM in the first 9 h were approximately 0.98 mg/h and 0.81 mg/h respectively. After 21 h, the average mass loss rates of FM and SM were approximately 1.95 mg/h and 1.63 mg/h respectively. It can be concluded that the average mass loss rate in the last 21 h was approximately twice that of the first 9 h, which might be due to excessive sputtering of the plasma on the mirror samples, where the Al_2O_3 deposition layer is completely removed in certain areas, exposing the Mo substrate which then continues to be sputtered by the Ar plasma. During the first 9 h, the mass loss was mainly due to the removal of the Al_2O_3 deposition layer. Over the subsequent 21 h, as the deposition layers were removed from more areas, the mass loss consisted of two contributions: the removal of the remaining Al_2O_3 deposition layers and the sputtering of the Mo substrate. Since the sputtering yields of Ar on Al and Mo are very close [20], while the mass numbers of Al and Mo differ significantly. This implies that when the number of sputtered Al and Mo particles is similar, the ratio of mass loss of Al to Mo is approximately 0.28, which is consistent with the experimental results.

Additionally, the measurement results show that after 30 h of cleaning, the average mass loss of samples 6, 7, 10, and 11 in the central area of FM is about 0.99 mg, while the average mass loss of samples 1, 4, 13, and 16 in the edge area was approximately 4.94 mg, which is almost 5 times that of the former. Similarly, the average mass loss of the four samples in the center area of the SM was 0.42 mg, and the average mass loss of the four samples in the edge area was 4.51 mg, which is more than 6 times the former. It can be observed that there is a significant difference in the cleaning uniformity between the edge and the central area in this experiment. Taking sample 7 located at the center of the SM as an example, after 30 h of cleaning, its mass loss was only approximately

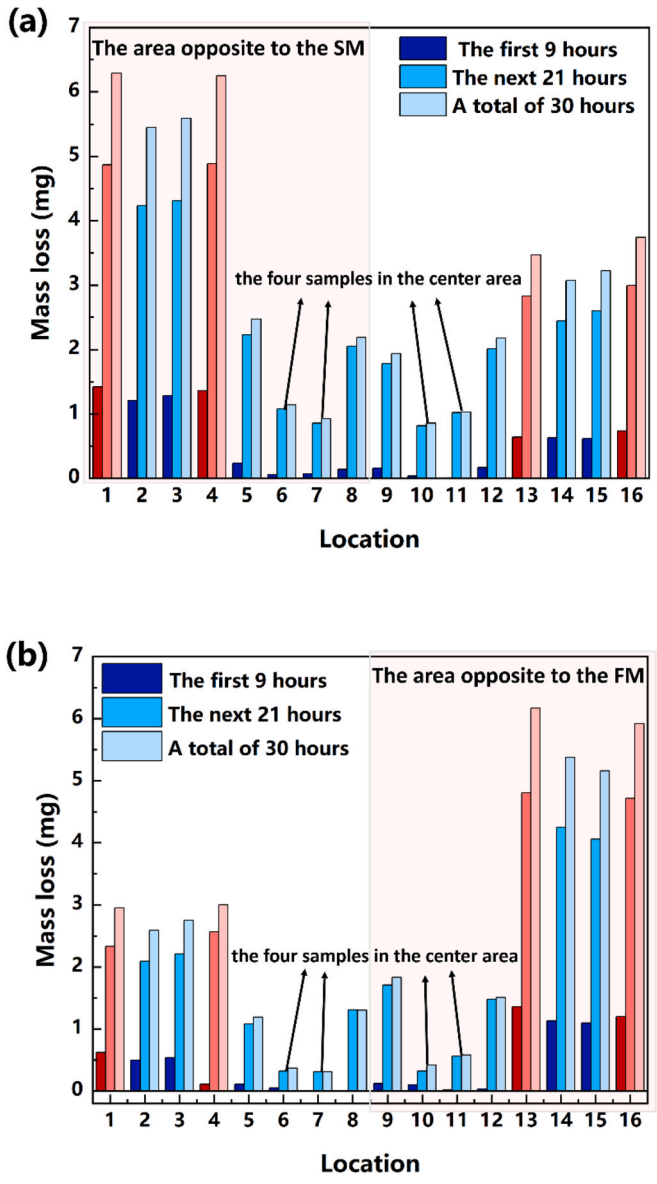

Fig. 10. Mass loss (mg) of samples on (a) FM and (b) SM before and after different cleaning times. (Red represents the four samples in the edge area, and the red rectangular area represents the regions where FM and SM are directly facing each other). (For interpretation of the references to colour in this figure legend, the reader is referred to the web version of this article.)

0.31 mg, which was much lower than that of the samples in the edge area. This indicates that under the current design, the cleaning efficiency in the central area is much lower than that in the edge area. Although the cleaning endpoint was not found in this experiment, the above mass loss data suggest that if the entire surface of the mirror needs to have the deposition layer completely removed, the edge area may be over-cleaned. This result indicates that the current geometric structure of the FMU still has deficiencies in achieving uniform cleaning, and the spacing and structural layout between the two mirrors in the FMU need to be further optimized in future designs. Furthermore, The significant difference in mass loss between the central and edge regions once again confirms the unevenness of the cleaning process mentioned in Section 3.1.

After a total of 30 h of RF plasma cleaning, the mass loss of the samples on FM and SM is shown in Fig. 10. The mirror samples within the red rectangular boxes on FM and SM are placed face-to-face in the FMU. After weighing and calculation, the average mass loss of the 1–8 samples directly facing SM on the FM was approximately 3.79 mg, while the average mass loss of the 9–16 samples in the non-directly-facing area was approximately 2.44 mg. The former was higher than the latter. Correspondingly, the average mass loss of the 9–16 samples on SM with respect to FM was approximately 3.37 mg, which was also higher than the 1.81 mg in the non-aligned area. The above experimental results indicate that the geometric structure of the FMU will affect the cleaning uniformity during the double mirror surface cleaning process, which will be analyzed in detail through PIC-MCC simulation in Section 3.3.

3.3. Erosion mechanisms

The experimental results in Section 3.1 and 3.2 demonstrate that the geometric structure of the FMU has a significant impact on the uniformity of cleaning: the mass loss in the regions directly opposite FM and SM is greater. Due to the limited diagnostic capabilities of the current experimental platform, such as the absence of Langmuir probes or ion energy analyzers, it is impossible to directly measure the ion flux and the distribution of ion energy. To assist in explaining the radio frequency discharge cleaning behavior observed in the experiment, this paper uses the PIC-MCC simulation method to conduct a numerical simulation of the Ar radio frequency discharge process in the FMU. The main purpose of the simulation is to obtain the ion flux distribution and ion energy distribution that are difficult to directly measure in the experiment, providing a physical explanation for the experimental results.

The PIC-MCC method is a commonly used approach in plasma simulations [20]. Its fundamental idea is to use a limited number of macroscopic particles to represent a large number of actual charged particles. The electromagnetic field is solved on a discrete spatial grid, and the motion of the macroscopic particles is tracked by solving the motion equations. Within each time step, the charge of the macroscopic particles is interpolated to obtain the charge density, the Poisson equation is solved to obtain the self-consistent potential and electric field distribution, and then the electric field is interpolated back to update the velocities and positions of the particles. After the particle advancement is completed, the Monte Carlo collision module based on experimental collision cross-section data processes various collisions (elastic scattering, excitation, ionization, charge exchange) between electrons, ions, and neutral gases through random sampling. Combining these two methods can be used to simulate complex plasma motions.

The discharge similarity laws (SLs) are of great significance for the correlation and prediction of plasma parameters at different scales. Yang et al. studied the similarity relationships in dual-frequency RF plasmas through a complete dynamic PIC/MCC simulation system, confirming that when the pressure p, discharge gap d, and driving frequency f simultaneously satisfy proportional scaling, even in the presence of electrical asymmetry effect (EAE), the key discharge characteristics such as electron density, ion density, ion flux, and ion energy distribution function remain consistent under similar conditions [21]. Based on the above similarity theory, in this simulation, the geometric dimensions of the experimental device were reduced by 0.5 times in proportion, and the gas pressure and radio frequency were correspondingly reduced from 1 Pa and 13.56 MHz to 0.5 Pa and 6.78 MHz, thereby ensuring that the simulation results are comparable to the experiments at the physical mechanism level while reducing the computational cost. During the geometric scaling process, the main structural features in the FMU were retained, including the two mirror electrodes, the grounding protection shells at both ends of the mirror, and the discharge space near the mirror (the black segments represent vacuum and the pink segments represent the grounded metal walls), as shown in Fig. 11. The simulation results can be compared with the experimental results based on the discharge similarity ratio [22].

FM and SM are set as RF driving electrodes and are connected to the voltage source through an external RF circuit. The two mirror electrodes were driven in phase (0° phase difference) as the baseline configuration, representing the most symmetric driving state for the dual-mirror

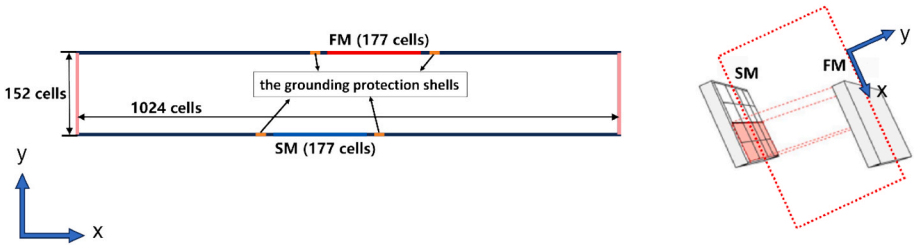

Fig. 11. PIC-MCC simulation setup diagram.

discharge. Ground protection shells are installed at both ends of the mirror surface, and the left and right boundaries are grounded metal walls with an electric potential fixed at 0 V. Except for the RF electrodes, the grounding protection shell and the left and right grounding metal walls, the remaining boundaries adopt vacuum boundary conditions. For charged particles, they are absorbed upon reaching the solid boundary; for the vacuum boundary, particles are removed after leaving the simulation area, and the electric potential along the vacuum boundary is assumed to be linearly varying. This is because we consider that the plasma space charge at the vacuum boundary in the simulation domain is relatively small and the structure is relatively simple. The electric field between the two end electrodes of the vacuum boundary is itself close to one-dimensional, so we adopted this linear variation assumption in order to obtain a boundary condition that is easier to handle. The potential at the boundary endpoints is equal to the potential of the adjacent electrodes. For the RF electrodes and the grounding metal walls, particles will bounce off the metal walls, generating elastic and inelastic reflected particles, and considering secondary electron emission. Among them, the proportion of elastic reflection of particles r_e-emitted from the wall after being incident on the wall by electrons is 0.03, and the proportion of inelastic reflection r_i is 0.07. The actual secondary electron emission coefficient is:

$$\gamma_t(\omega, \theta) = (1 - r_e - r_i)\gamma_V(\omega, \theta) \tag{3.1}$$

In our simulation, the energy threshold for elastic electron collisions on the radio frequency electrode was set at 2 eV. The incident energy corresponding to the maximum emission when the incident light is perpendicular was set at 10 eV, and the maximum emission coefficient was 0.55. The energy threshold for electron-induced secondary electron emission was 13 eV. When the incident light is perpendicular, the corresponding incident energy was set at 500 eV, and the maximum emission coefficient was 3, with a smoothness factor of 1.0. When ions collide with the wall, they are completely absorbed by the wall. If the energy is between 100 eV and 10,000 eV, it will induce secondary electron emission with an emission coefficient of 0.2, and the temperature of the emitted electrons is 2 eV. On the grounded metal wall, electron pure absorption is set, and there is no real secondary particle emission.

The radio frequency electrode potential is obtained by solving the external circuit model. This approach is based on the method proposed by Vahedi and DiPeso for simultaneously solving the potential and the external circuit in the two-dimensional bounded PIC simulation [23]. In the simulation, the working gas is Ar gas. The neutral Ar atoms are treated as a uniform background gas, with a temperature of 300 K. The pressure is set at 0.5 Pa. Elastic, inelastic and ionization collisions between electrons and Ar atoms are considered, among which only primary ionization is considered for ionization collisions. At the initial moment, the electron density and ion density are 3×10^{13} m^{-3}, the electron temperature is 4 eV, and the ion temperature is 300 K. Among them, the electron temperature of 4 eV is within the typical range of low-pressure capacitive coupling radio frequency discharge (1–5 eV) [24]. The ion temperature of 300 K is consistent with the typical value of ion temperature in this type of plasma (in the order of hundreds of K) [25] based on the assumption of thermal equilibrium between the initial ions and the room-temperature neutral gas. Initially, we attempted to set the initial electron density and ion density as 2.41×10^{15} m^{-3}, 5×10^{14} m^{-3} and 3×10^{13} m^{-3}. The results showed that both the steady-state electron density and ion density were at the order of 10^{14} m^{-3}. Therefore, the initial electron density and ion density of 3×10^{13} m^{-3}, which is slightly less than the steady-state value, were finally selected. The grid cell step size used in the simulation is 1/3 of the initial Debye length of the plasma electrons, the time step size is 0.23 ns, the number of particles per grid is 200, the total simulation time is 10000 ns, which is approximately 68 radio frequency cycles. Subsequently, the data of the last 6.8 RF cycles are averaged in time to obtain a stable potential distribution, plasma density, ion flux and ion energy distribution. Indeed, the simulation parameters were not exactly the same as the experiment. The results can still be of reference.

The simulation reached quasi-steady state after approximately 900 time steps, as shown in Fig. 12. The self-bias voltages of FM and SM were both respectively stabilized at approximately −298 V, which were highly consistent with the experimentally preset −300 V.

From the spatial distribution maps of FM and SM ion fluxes shown in Fig. 13, it can be observed that the ion flux in the edge region is significantly higher than that in the central region. This is due to the influence of the grounded metal protective shell on the edge of the mirror, as shown in Fig. 14. A transverse electric field component was generated at the edge of the mirror close to the grounded protective shell. This electric field attracted ions to both the FM and SM ends, resulting in an increase in the ion density in the edge area and a corresponding increase in the ion flux. This non-uniform distribution directly leads to more ion bombardment in the edge region, thereby causing more atomic layers to be sputtered off, and macroscopically, it is manifested as the same cleaning time, the mass loss in the edge region being higher than that in the central region[26]. The overall trend of the measured mass loss distribution is consistent with the ion flux distribution obtained from the simulation. The mass loss in the edge region is indeed higher than that in the central region. However, quantitative comparison reveals that the ion flux at the edge is approximately 1.7 times that at the center, but the average mass loss at the edge is 5–6

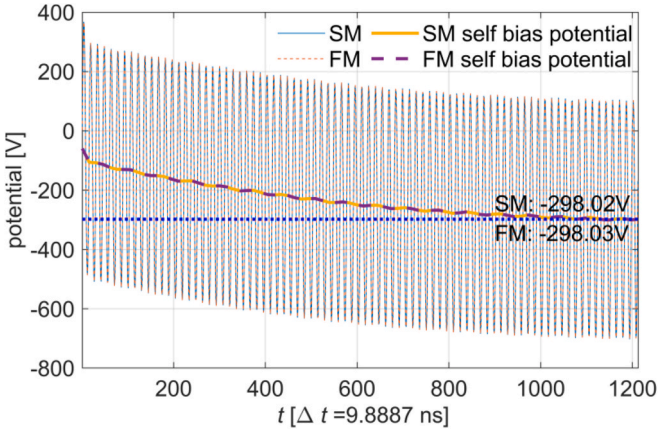

Fig. 12. The variations of the self-bias voltages of FM and SM over time.

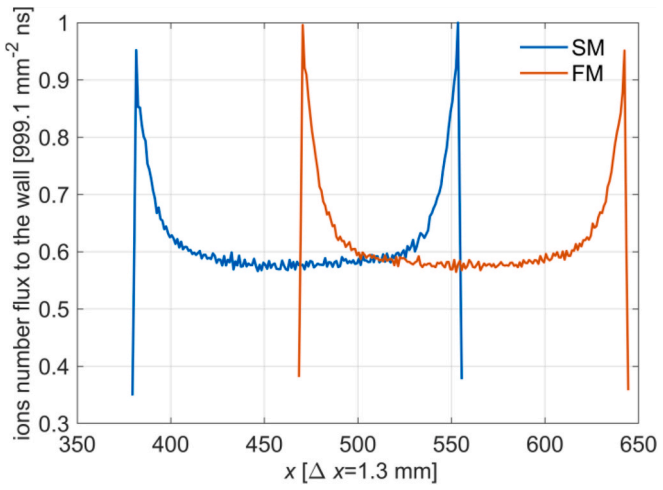

Fig. 13. The fluxes of FM and SM ion numbers (averaged from step 1000 to step 1200).

times that at the center. This significant difference cannot be solely explained by the difference in ion flux. Additionally, it is necessary to consider that the edge region undergoes excessive sputtering described in Section 3.1, thereby causing the mass loss in the edge region to be significantly amplified.

From the ionization rate distribution in Fig. 15, it can be seen that the positive alignment area between FM and SM has a significantly higher ionization rate than other areas. The increase in ionization rate leads to an increase in the ion density in this area. Under the same sheath layer acceleration conditions, more ions are extracted and bombarded by the mirror [27]. Therefore, the mass loss in the positive alignment area of the two mirrors is greater than in other positions.

We emphasize that the primary value of the PIC-MCC simulation in this study lies in revealing the physical processes that are difficult to directly measure in experiments, providing a physical mechanism explanation for the non-uniform cleaning phenomenon observed in the experiments, rather than replacing experiments for quantitative predictions. The consistency of the simulation results with the experimental data in terms of trend, that is, the ion flux at the edge of the mirror is higher than that at the center, and the ionization rate increases in the two mirror-facing regions, is sufficient to support our physical inference of the cleaning non-uniformity. The PIC-MCC simulation is mainly used as a mechanism explanation tool, rather than a prediction model.

4. Conclusion

In this study, two face-to-face arranged first mirrors were cleaned by Ar RF plasma under 1 Pa gas pressure and − 300 V uniform self-bias for a total of 30 h (9 h + 21 h staged cleaning). Combined with material characterization and PIC-MCC numerical simulation, the cleaning efficiency and spatial uniformity of double-mirror synchronous cleaning were investigated, and the main conclusions are summarized as follows.

(1) After 30 h of plasma treatment, the Al_2O_3 contaminant layer simulating Be deposition was fully removed from both mirrors, with Al and O contents reduced to zero according to EDS analysis. The reflectivity of the typical position reflector sample has basically returned to its original state, for example, the total reflectiivity of sample 5 on the FM at the wavelength of 800 nm recovered from approximately 25% before cleaning to approximately 65% after cleaning, with an absolute increase of 40 percentage points. verifying the feasibility of RF plasma cleaning for dual opposed mirrors.

(2) Obvious asymmetric non-uniform cleaning distribution exists on both mirrors. The material mass loss at mirror corners and edges is 5–6 times larger than that in the central area, and serious over-sputtering of Mo substrate occurs at edge positions. The uneven distribution of ion fluxes is the primary cause of the non-uniform cleaning at the edges and the center, meanwhile, impurity re-deposition in central zones further lowers the central cleaning efficiency.

It should be noted that the 30-hour cleaning duration in this study was a fixed total time that was pre-set without conducting real-time endpoint monitoring. Therefore, after the Al_2O_3 deposition layer was completely removed, the cleaning process continued, resulting in unnecessary sputtering of the Mo substrate, especially more pronounced in the edge areas. Although this limitation exists, the extended cleaning period does not affect the validity of the findings in this study regarding the uneven cleaning in the edge and center regions. Additionally, the optical properties of FM and SM have been significantly restored compared to their pre-cleaning state.

(3) The geometric relative position of the two mirrors strongly affects cleaning uniformity. Experimental data shows the directly opposite region of two mirrors achieves higher cleaning removal capacity. PIC-MCC simulation confirms that the overlapping discharge between opposed mirrors improves the ionization rate in the intermediate gap, raising local ion density and bombardment flux and consequently accelerating sputtering removal at facing regions. It should be noted that the PIC-

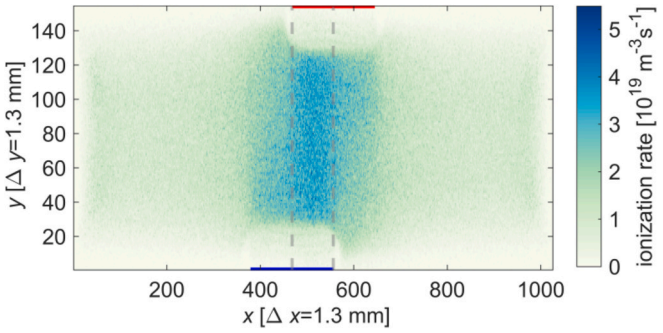

Fig. 15. The ionization rate distributions of FM and SM (averaged over time from step 1201 to step 1212).

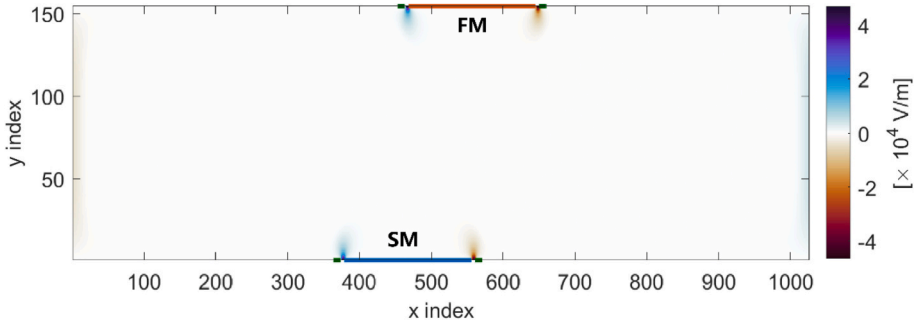

Fig. 14. The graph of the x-component of the electric field (averaged over the last 200 steps).

MCC simulation in this study is mainly used as a qualitative tool for explaining the physical mechanism, rather than a quantitative prediction model. The simulated ion flux distribution and ionization rate are consistent with the experimental trends, but have not yet been quantitatively verified against the measured data. Future work will focus on on-site diagnosis to achieve the quantitative verification of the simulation results.

The present work clarifies the non-uniform cleaning law of face-to-face dual mirrors and its microscopic physical mechanism. The obtained experimental conclusions and simulation data can serve as a reference for the in-situ cleaning of FMs and the structural design of the FMU in future fusion reactor devices. For instance, perhaps the FMs could be designed in other shapes, such as a circle; In addition, optimize the spacing and structural layout between the mirrors in the FMU. These ideas still need to be further verified through more subsequent experiments. Further optimization on electrode layout and discharge parameters will be carried out in follow-up research to restrain excessive edge etching and improve overall cleaning homogeneity.

CRediT authorship contribution statement

Yuxian Wen: Writing – original draft, Methodology, Investigation, Data curation, Conceptualization. **Rong Yan:** Writing – review & editing, Supervision, Project administration, Methodology, Funding acquisition, Conceptualization. **Chuannan Xuan:** Writing – review & editing, Supervision, Conceptualization. **Lei Mu:** Methodology, Investigation. **Yuming Liu:** Methodology, Investigation. **Yuhao Pan:** Methodology, Investigation, Conceptualization. **Zhaohui Wang:** Methodology, Investigation. **Baoguo Wang:** Methodology, Investigation. **Shuyue Sun:** Methodology, Investigation. **Rui Ding:** Writing – review & editing, Data curation. **Andrey Litnovsky:** Writing – review & editing, Methodology. **Junling Chen:** Resources, Project administration, Funding acquisition.

Declaration of competing interest

The authors declare that they have no known competing financial interests or personal relationships that could have appeared to influence the work reported in this paper.

Acknowledgement

This work was supported by the National key R&D project of China with project number of 2024YFE03000200, 2022YFE03030000, and 2024YFE03160004, the National Nature Science Foundation of China under Contract Nos. 12522515, 12275306, 11975269, U24A2020, and 12075279, the Youth Innovation Promotion Association of Chinese Academy of Sciences under certificate No. 2022452, the Anhui Provincial Natural Science Foundation under contract 2208085 J40, the Anhui Provincial Major Science and Technology Project under contract No. E35AH205B3, the CASHIPS Director's Fund with Grant Nos. BJPY2023B03, YZJJQY202302, and BJPY2023A03. We gratefully thank the vacuum group members at EAST for their valuable support. We also thank the staff members at EAST (https://cstr.cn/31130.02.EAST), for providing technical support and assistance in data collection and analysis.

Data availability

Data will be made available on request.

References

[1] E.E. Mukhin, V.V. Semenov, A.G. Razdobarin, et al., First mirrors in ITER: material choice and deposition prevention/cleaning techniques, Nucl. Fusion 52 (013017) (2012).
[2] L. Moser, L. Marot, R. Steiner, et al., Plasma cleaning of ITER first mirrors, Phys. Scr. T170 (014047) (2017).
[3] J. Chen, R. Yan, J.L. Chen, Influence of erosion and Deposition on Metallic first Mirror in HT-7 Tokamak, Plasma Science & Technology 14 (2012) 708–711.
[4] A. Litnovsky, Y. Krasikov, V. Kotov, et al., Mirror Station for studies of the protection of diagnostic mirrors from impurity contamination in ITER: Design and first results, Fusion Eng. Des. 96–97 (2015) 290–293.
[5] J. Rapp, G.J. van Rooij, A. Litnovsky, et al., Temperature effect on hydrocarbon deposition on molybdenum mirrors under ITER-relevant long-term plasma operation, Phys. Scr. T138 (014067) (2009).
[6] A. Litnovsky, V. Philipps, P. Wienhold, et al., Active control over carbon deposition on diagnostic components and in remote areas of ITER, J. Nucl. Mater. 417 (2011) 830–833.
[7] A.G. Razdobarin, A.M. Dmitriev, A.N. Bazhenov, et al., RF discharge for mirror surface recovery in ITER, Nucl. Fusion 55 (093022) (2015).
[8] L. Moser, L. Marot, R. Steiner, et al., Plasma cleaning of beryllium coated mirrors, Phys. Scr. T167 (014069) (2016).
[9] A. Litnovsky, D.L. Rudakov, G. De Temmerman, et al., First tests of diagnostic mirrors in a tokamak divertor: an overview of experiments in D111-D, Fusion Eng. Des. 83 (2008) 79–89.
[10] J. Peng, R. Yan, J.L. Chen, et al., Study on plasma cleaning of the large-scale first mirror of the charge exchange recombination spectroscopy diagnostic on EAST, Plasma Science & Technology 22 (034004) (2020).
[11] M. Rubel, D. Ivanova, J.P. Coad, et al., Overview of the second stage in the comprehensive mirrors test in JET, Phys. Scr. T145 (014070) (2011).
[12] D.L. Rudakov, C.P.C. Wong, A. Litnovsky, et al., Overview of the recent DiMES and MiMES experiments in DIII-D, Phys. Scr. T138 (014007) (2009).
[13] S. Moon, P. Petersson, M. Rubel, et al., First mirror test in JET for ITER: complete overview after three ILW campaigns, Nucl. Mater. Energy 19 (2019) 59–66.
[14] A. Litnovsky, M. Matveeva, A. Herrmann, et al., First studies of ITER-diagnostic mirrors in a tokamak with an all-metal interior: results of the first mirror test in ASDEX Upgrade, Nucl. Fusion 53 (073033) (2013).
[15] M. Rubel, G. De Temmerman, P. Sundelin, et al., An overview of a comprehensive first Mirror Test for ITER at JET, J. Nucl. Mater. 390–91 (2009) 1066–1069.
[16] D. Samsonov, A. Kamshilin, G. Marinin, et al., ITER-Relevant first Mirrors Unit with Integrated Mirror cleaning System Utilizing Capacitive coupled RF Discharge, IEEE Trans. Instrum. Meas. 73 (2024).
[17] P. Shigin, N. Babinov, G. De Temmerman, et al., RF discharge mirror cleaning system development for ITER diagnostics, Fusion Eng. Des. 164 (2021).
[18] A. Ushakov, C. Meekes, U. Stephan, et al., Performance study and comparison of vacuum RF circuits developed for first mirror plasma cleaning systems in ITER optical diagnostics, Fusion Eng. Des. 216 (2025).
[19] C.X. Wang, R. Yan, Y.M. Liu, et al., Cleaning of two mirrors in the first mirror unit using radiofrequency capacitively coupled plasma, Plasma Science & Technology 26 (2024).
[20] K. Matyash, R. Schneider, F. Taccogna, et al., Particle in cell simulation of low temperature laboratory plasmas, Contrib. Plasma Phys. 47 (2007) 595–634.
[21] D. Yang, H.H. Wang, B.C. Zheng, et al., Application of similarity laws to dual-frequency capacitively coupled radio frequency plasmas with the electrical asymmetry effect, Plasma Sources Science & Technology 31 (2022).
[22] J.Y. Sun, J. Schulze, F.F. Ma, et al., Similarity laws for two-dimensional simulations of low-pressure capacitively coupled radio-frequency discharges, Phys. Plasmas 30 (120702) (2023).
[23] V. Vahedi, G. DiPeso, Simultaneous potential and circuit solution for two-dimensional bounded plasma simulation codes, J. Comput. Phys. 131 (1997) 149–163.
[24] M.J. van de Sande, R.H.M. Deckers, F. Lepkojus, et al., Time resolved electron density and temperature measurements measurements on a capacitively coupled helium RF discharge, Plasma Sources Science & Technology 11 (2002) 466–475.
[25] G.A. Hebner, A.M. Paterson, Ion temperature and velocity in a 300 mm diameter capacitively coupled plasma reactor driven at 13, 60 and 162 MHz, Plasma Sources Science & Technology 19 (2010).
[26] A. Lopez-Cazalilla, C. Cupak, M. Fellinger, et al., Comparative study regarding the sputtering yield of nanocolumnar tungsten surfaces under Ar irradiation, Phys. Rev. Mater. 6 (075402) (2022).
[27] Y.L. Yu, Z.L. Zhang, Q.Y. Nie, et al., Electron dynamics and metastable species generation in atmospheric pressure non-equilibrium plasmas controlled by dual LF-RF frequency discharges, Front. Phys. 11 (1137250) (2023).